16th World Congress in Computational Mechanics (WCCM)
21-26 July 2024, Vancouver, Canada
A. Korobenko, M. Laforest, S. Prudhomme, R. Vaziri (Eds)

BEYOND LUBRICATION FLOW FOR THIN-FILM MANUFACTURING

ROBERT B. SECOR[1], REKHA RAO[2] AND WESTON ORTIZ[3]

[1]Center for Micro Engineering Materials, University of New Mexico
MSC04-2790, Albuquerque, NM 87131
rsecor59@unm.edu

[2] Engineering Science Center, Sandia National Laboratories*
P. O. Box 5800, Albuquerque, NM 87185
rrrao@sandia.gov

[3] Center for Micro Engineering Materials, University of New Mexico
MSC04-2790, Albuquerque, NM 87131
wortiz@unm.edu

Key words: Lubrication, FEM, Level-Set, non-Newtonian, Manufacturing.

Abstract. *Reynolds' hydrodynamic lubrication theory has been used extensively to analyze and quantify thin film manufacturing[1]. Applications span liquid flows in bearings, coatings, and molds, and gas flows between rigid or elastic surfaces. To enable further applications of efficient, reduced-order modelling, we pursue streamlined algorithms for non-Newtonian liquids in marginally "thin" geometries with multiple phases and capillarity. The goal is expanded use of "modified", non-traditional lubrication methods to bring physics-based knowledge to bear in process design, optimization, and control methods.*

Reynolds' lubrication applies to Newtonian fluids through thin flow channels. Accommodation for non-Newtonian flow behavior via generalized Newtonian constitutive relations can be achieved with the aid of variable transformations. The known stress-rate relation for a particular non-Newtonian rheological model can be transposed to yield pressure-drop/flowrate relationships of non-Newtonian lubrication flow. For non-moving boundaries, non-Newtonian lubrication can be formulated as one mass conservation and one momentum balance equation. When one or more channel boundaries are moving, the momentum balance expands to three equations to fully capture the shear-rate coupling between different momentum transport mechanisms.

For marginally high aspect-ratio flow channels, side walls exert significant drag on the flow that is not present in Reynolds' theory. An effectively lower liquid permeability instituted through a wall distance function suitably captures sidewall drag. Liquid-gas interfaces in filling applications are captured using level set tracking. Surface tension forces for high and medium Capillary Number flows are an additional lubrication modification. By combining an analytical thickness direction curvature with an in-plane level-set curvature field, wetting and de-wetting behavior are added to reduced-order lubrication modeling.

Non-Newtonian rheology, sidewall drag, and capillary forces are added to make a "modified" lubrication model. The resulting reduced dimensionality (3D flow problems are

reduced to 2.5D) promises a "step change" in model efficiency leading to increased capability for model size and complexity. We demonstrate this reduced order method on the flow of Newtonian and shear-thinning liquids through a patterned channel and find good agreement compared to a fully three-dimensional approach.

1 INTRODUCTION

Coarse-graining or reduced-order modelling of liquid flows in manufacturing almost always relies on Reynolds' hydrodynamic lubrication theory. Lubrication here refers to flowing liquid through thin channels, that is, one channel dimension, the gap, is much smaller than the other two, length and width. The bounding surfaces that form the thin channel can be rigid or deformable. Reynolds' lubrication considers isothermal, Newtonian flow through the thin channel and finds application in coating, bearing, calendaring, and film extrusion flows as well as filling molds and other cavities. For incompressible flow through a channel of gap, H(x,y), and impenetrable upper and lower boundaries, it has the following form.

$$\boldsymbol{\nabla}_{\boldsymbol{II}} \cdot \left[-\frac{H^3}{12\mu} \boldsymbol{\nabla}_{\boldsymbol{II}} p + \frac{H}{2} (\boldsymbol{U} + \boldsymbol{V}) \right] = 0 \tag{1}$$

Here μ is the Newtonian viscosity and p is the liquid pressure, while the geometry is depicted in Figure 1. The lubrication plane is a x-y plane in a x-y-z Cartesian coordinate system spanning the width and length of the channel. The two-dimensional lubrication plane gradient, $\boldsymbol{\nabla}_{\boldsymbol{II}} \equiv \boldsymbol{i}\frac{\partial}{\partial x} + \boldsymbol{j}\frac{\partial}{\partial y}$, is the gradient in the lubrication plane and the z-coordinate spans the channel gap perpendicular to the lubrication plane. **U** and **V** are the vector velocities of the upper and lower surfaces in the lubrication plane.

Roberts et al.[1] described expansions to Reynolds' lubrication in applications to multiphase flow using a three-dimensional shell finite element method. The level-set method captured liquid-gas interfaces between phase regions in the channel and a continuous surface force tensor formulation quantified interfacial forces. In addition, fluid-structural interactions were captured between the lubrication flow and elastic deformation of the solids forming the channel.

We propose further expansions of lubrication methods in the areas of non-Newtonian rheology and "not so" thin or wide channels in a similar multiphase context. The goal is to create efficient algorithms for applications technically beyond the confines of lubrication to bring physics-based knowledge to the design, optimization, and control of complicated manufacturing processes.

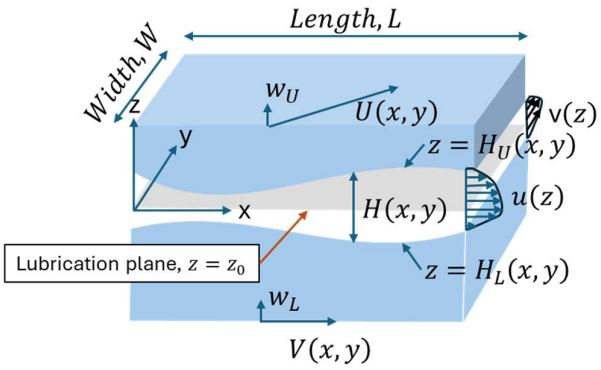

$$\boldsymbol{e_i} = \boldsymbol{i}, \boldsymbol{j}, \boldsymbol{k} \qquad \boldsymbol{e_{II}} \equiv \boldsymbol{ii} + \boldsymbol{jj}\,, \boldsymbol{\nabla_{II}} \equiv \boldsymbol{i}\frac{\partial}{\partial x} + \mathbf{j}\frac{\partial}{\partial y}$$

Figure 1: Lubrication flow geometry.

2 GENERALIZED NEWTONIAN LUBRICATION

Reynolds' lubrication theory is restricted to Newtonian flow where the fluid viscosity is constant. Generalized Newtonian constitutive relations accommodate viscosity functions that depend on the local deformation rate, but in lubrication analyses the local deformation rate is not known a priori. Fortunately, the known stress-rate relationship inherent in the Generalized Newtonian constitutive relation can be utilized via variable transformations to deduce the overall flowrate vs. pressure gradient relationship, i.e., the "flow curve".[2] The flow curve for Generalized Newtonian fluids bears a striking resemblance to their viscosity curve, i.e., the viscosity vs. shear rate dependence, if it is scaled appropriately. An example is shown in Figure 2 for a Carreau-Yasuda fluid (cf. Bird et al., p. 171).[3] This similarity suggests a direct relationship between the two. The shear stress exerted on the walls of a thin channel is directly related to the flow direction pressure gradient,

$$\tau_w = \frac{H}{2}|\boldsymbol{\nabla_{II}} P|. \tag{2}$$

Here $\nabla_{II} P$ is the pressure gradient in the plane of the thin channel, where P is the liquid pressure modified for the effect of gravity. Under lubrication conditions, any flow perpendicular to the channel plane is quite small in relation to the length and width direction consistent with very small pressure variation in the thickness direction, i.e., $\frac{dP}{dz} \approx 0$. The flow vector, $\boldsymbol{q} \equiv \int \boldsymbol{v_{II}} dz$, is the integrated fluid velocity across the channel gap and is sensibly the flowrate per unit width through the channel. Since it is directly related to fluid velocity, there is only an indirect relationship to the shear rate in the channel. Integration by parts applied to the flow vector definition makes this clearer,

$$\boldsymbol{q} = \boldsymbol{v_{II}}|_{z=H_L}^{z=H_U} - \int z \frac{\partial \boldsymbol{v_{II}}}{\partial z} dz \tag{3}$$

The subscripts U and L refer to the upper and lower bounding surfaces of the lubrication channel. Sensibly the local shear rate in the channel will be small in the center of the channel and have the highest magnitude at the channel walls. As the degree of liquid shear-thinning increases, the wall shear rate also increases for a given flowrate. The magnitude of the flow

vector is strongly correlated with wall shear rate, but the precise relationship depends on the viscosity function and magnitude of stress causing the flow, i.e., wall shear stress or channel pressure gradient.

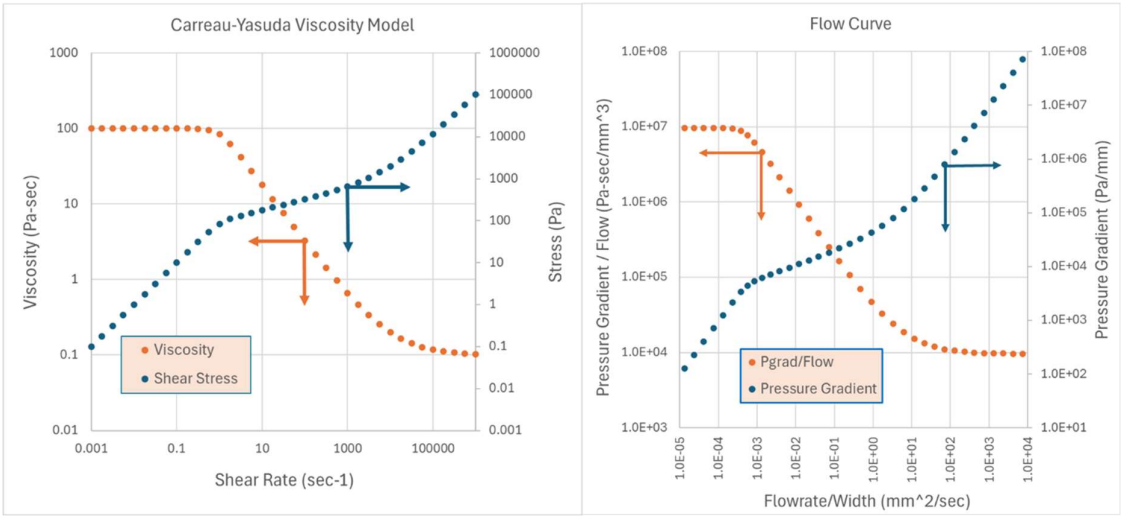

Figure 2 – Comparison of the viscosity curve (left) of a Carreau-Yasuda fluid to the corresponding flow curve (right) in a thin channel. The Carreau-Yasuda parameters are η_0=100 Pa-sec, n=0.25, λ=1.0 sec, p=3, and η_∞=0.1 Pa-sec. The flow curve is calculated for a channel gap of 0.050 mm.

2.1 One-dimensional Generalized Newtonian Lubrication Flow

Fortunately, the precise flow curve relationship for Generalized Newtonian fluids can be deduced from the viscosity function and mass and momentum balances integrated across the lubrication channel gap. For incompressible flow, the integrated conservation of mass (also volume) proceeds as follows.

$$\int_{H_L}^{H_U}\left[\frac{\partial\rho}{\partial t}+\rho\nabla\cdot\boldsymbol{v}\right]dz=0=H\frac{\partial\rho}{\partial t}+\rho\left[\boldsymbol{\nabla_{II}}\cdot\int_{H_L}^{H_U}\boldsymbol{v_{II}}dz\right]=H\frac{\partial\rho}{\partial t}+\rho\boldsymbol{\nabla_{II}}\cdot\boldsymbol{q} \tag{4}$$

Here H is the lubrication channel gap, $H\equiv H_U(x,y)-H_L(x,y)$, and $\boldsymbol{v}(x,y,z)$ is the general three-dimensional velocity field while $\boldsymbol{v_{II}}(x,y)$ refers to dominant velocity in the lubrication plane, i.e., ignores the v_z component. The channel walls, located at $z=H_U(x,y)$ and $z=H_L(x,y)$, have been assumed to be impenetrable above. Likewise, under lubrication conditions, i.e., thin channel and only modest gap changes, the lubrication plane momentum balance has the following form

$$(z-z_0)\boldsymbol{\nabla_{II}}P=\boldsymbol{\tau}_{z,II}=\eta(|\boldsymbol{L}(z)|)\boldsymbol{L}(z),\boldsymbol{L}\equiv\frac{\partial\boldsymbol{v_{II}}}{\partial z}\ \ or\ \ H\boldsymbol{\nabla_{II}}P=\eta(|\boldsymbol{L}_U|)\boldsymbol{L}_U-\eta(|\boldsymbol{L}_L|)\boldsymbol{L}_L \tag{5}$$

z_0 is the location of the lubrication plane and L is the out-of-plane velocity gradient, which is the dominant component. The in-plane components, $L_{II,II}$, are sensibly of much lower magnitude given the channel dimensions.

If the walls of the lubrication channel are stationary in the lubrication plane, the flow within is one-dimensional. The only driving force for flow is the pressure gradient and the flow must

be directed in the opposite direction to that of the pressure gradient, denoted by the unit vector $\boldsymbol{e}$ below and the scalar L is the velocity gradient magnitude.

$$\boldsymbol{q} = -q\boldsymbol{e}\,, \qquad \boldsymbol{e} \equiv \frac{\boldsymbol{\nabla_{II}} P}{|\boldsymbol{\nabla_{II}} P|}, \qquad L = |\boldsymbol{L}| = \sqrt{\left(\frac{\partial}{\partial z}\boldsymbol{i}\cdot\boldsymbol{v_{II}}\right)^2 + \left(\frac{\partial}{\partial z}\boldsymbol{j}\cdot\boldsymbol{v_{II}}\right)^2} \tag{6}$$

The flow is symmetric in the gap direction and velocity gradient at the upper and lower surfaces are equal in magnitude and opposite in sign.

$$\boldsymbol{q} = -\int_{H_L}^{H_U} z\frac{\partial \boldsymbol{v_{II}}}{\partial z}\,dz\,, \quad q = -2\int_0^{\frac{H}{2}} L z dz\,, \;\; H|\boldsymbol{\nabla_{II}} P| = 2\eta(L_w)L_w \tag{7}$$

Through a variable transformation from the gap coordinate to shear stress to velocity gradient, $z \to \tau \to L$, the flow in response to pressure gradient can be reduced to a simple correspondence through the wall shear rate, L_w.

$$\begin{aligned} q = -2\int_0^{\frac{H}{2}} L z dz &= -\frac{H^2}{2\tau_w^2}\int_0^{\tau_w} L\tau d\tau = -\frac{H^2}{2\tau_w^2}\int_0^{L_w} \eta L^2\left(\eta + L\frac{d\eta}{dL}\right)dL \\ &= -\frac{H^2}{4}\left[L_w - \frac{1}{\tau_w^2}\int_0^{L_w}\eta^2 L^2 dL\right] \end{aligned} \tag{8}$$

If the viscosity integral is made dimensionless, the connection between flowrate and wall shear rate, and indirectly pressure gradient is, perhaps, simpler.

$$\tilde{I} \equiv \frac{1}{L_w\tau_w^2}\int_0^{L_w}\eta^2 L^2 dL = \frac{1}{\eta_w^2}\int_0^1 \eta(\xi L_w)^2\xi^2 d\xi\,, \qquad q = -\frac{H^2}{4}L_w[1-\tilde{I}] \tag{9}$$

As a result, Reynolds' lubrication modified for generalized Newtonian models for the special case of stationary walls and incompressible flow becomes as follows.

$$\boldsymbol{\nabla_{II}}\cdot\left[-\frac{H^2 L_W}{4}\left(1 - \frac{1}{\eta_w^2}\int_0^1 \eta(\xi L_w)^2\xi^2 d\xi\right)\right] = 0, \;\; \eta(L_w)L_w = \frac{H}{2}|\boldsymbol{\nabla_{II}} P| \tag{10}$$

For several Generalized Newtonian constitutive relations, e.g., power-law, Herschel-Buckley, and Carreau-Yasuda with the exponent p=3, the integral in (9) is available analytically. For others, it can be numerically evaluated using Gaussian quadrature or other similar techniques.

2.2 Two-dimensional Generalized Newtonian Lubrication Flow

When the channel walls are moving, the flow is, in general, two-dimensional. In addition to the pressure gradient driving force, the walls drag fluid in potentially different directions. It is useful to define a second direction, $\boldsymbol{f}$, perpendicular to the pressure gradient direction, $\boldsymbol{e}$, defined in (6).

$$\boldsymbol{e}\cdot\boldsymbol{f} = 0, \qquad \boldsymbol{L} \equiv \frac{\partial \boldsymbol{v_{II}}}{\partial z} = \mathbf{e}\mathrm{L_e} + \mathbf{f}\mathrm{L_f}, \qquad L_e = \frac{\partial \boldsymbol{e}\cdot\boldsymbol{v_{II}}}{\partial z}, \;\; \mathrm{L_f} = \frac{\partial \boldsymbol{f}\cdot\boldsymbol{v_{II}}}{\partial z} \tag{11}$$

The flow is not symmetric in the gap direction, but the momentum balance (5) still applies. Since there is no pressure gradient in the $\boldsymbol{f}$ direction, the shear stress in that direction is constant across the lubrication channel gap and determines how the two velocity gradients, L_e and L_f are related. The no-slip boundary condition at the bounding surfaces, shown here in integral form,

together with the stress balance complete the governing equations.

$$\boldsymbol{f}\cdot\boldsymbol{\tau}_{\boldsymbol{z,II}} = \mathrm{K} = \eta\left(L_e, L_f\right)\mathrm{L_f}, \qquad \mathbf{U}-\mathbf{V} = \int_{H_L}^{H_U} \boldsymbol{L}dz \tag{12}$$

Like the one-dimensional flow situation, a variable transformation from the gap coordinate to shear stress to velocity gradient, $z \to \tau \to L$, converts the momentum balance and no-slip condition to functions of the surface velocity gradients.

$$(\boldsymbol{U}-\boldsymbol{V})|\boldsymbol{\nabla_{II}}P| = \mathbf{e}\left[\eta\left(L_e, L_f\right)L_e^2\Big|_L^U - \int_{L_e^L}^{L_e^U}\eta L_e dL\right] + \mathbf{f}\mathrm{K}\left[L_e(1+\ln\eta)\Big|_L^U - \int_{L_e^L}^{L_e^U}\ln\eta\, dL\right] \tag{13}$$

$$\boldsymbol{q} = \frac{\boldsymbol{U}\eta L_e^U - \boldsymbol{V}\eta L_e^L}{|\boldsymbol{\nabla_{II}}P|} = \frac{1}{|\boldsymbol{\nabla_{II}}P|^2}\left\{\frac{\mathbf{e}}{\mathbf{2}}\left[\eta^2 L_e^3\Big|_L^U - \int_{L_e^L}^{L_e^U}\eta^2 L_e^2 dL\right] + \mathbf{f}\mathrm{K}\left[\eta^2 L_e^2\Big|_L^U - \int_{L_e^L}^{L_e^U}\eta L_e dL\right]\right\} \tag{14}$$

The flow vector expression (14) captures the flowrate pressure drop relationship in the general, moving boundary situation, while the two components of the no-slip conditions (13) and momentum balance (12) provide governing equations for the quantities K, L_e^U, and L_e^L that the flow vector depends on.

3 NOT SO WIDE, THIN FLOW CHANNELS

Often molds to be filled have obstacles in the flow path or stripes and discontinuous coatings may be applied to a substrate. Applications like these feature flow passages that are not so wide with aspect ratios as low as unity. Section 5 below shows two examples in Figures 5 and 6. The side walls in the narrow passages exert extra drag on the flow, causing lubrication calculations to underpredict the pressure difference for a given flowrate (or overpredict flowrate for a given pressure gradient). For Newtonian liquids, the side wall effect is usually accessible analytically. For example, the velocity field in a rectangular channel can be represented as an infinite series[4].

$$u(y,z) = \frac{\Delta p}{L}\frac{H^2}{8L}\left\{1 - 4\frac{z^2}{H^2} - \sum_{n=0}^{\infty}\frac{32(-1)^n\cosh(2n+1)\pi\frac{y}{H}\cos(2n+1)\pi\frac{z}{H}}{(2n+1)^3\pi^3\cosh(2n+1)\pi\frac{W}{2H}}\right\} \tag{15}$$

L is the channel length and W its width. The effective local permeability across the channel, that is, the ratio of flow to pressure gradient scaled with viscosity, comes from the integrated velocity profile across the channel gap. The local permeability in series form is as follows and is shown in Figure 3.

$$q(y) = \int_{-\frac{H}{2}}^{\frac{H}{2}} u(y,z)dz \to \frac{q(y)}{\nabla p}\mu = \frac{H^3}{12}\left[1 - \frac{3}{2}\sum_{n=0}^{\infty}\frac{64\cosh(2n+1)\pi\frac{y}{H}}{(2n+1)^4\pi^4\cosh(2n+1)\pi\frac{W}{2H}}\right] \tag{16}$$

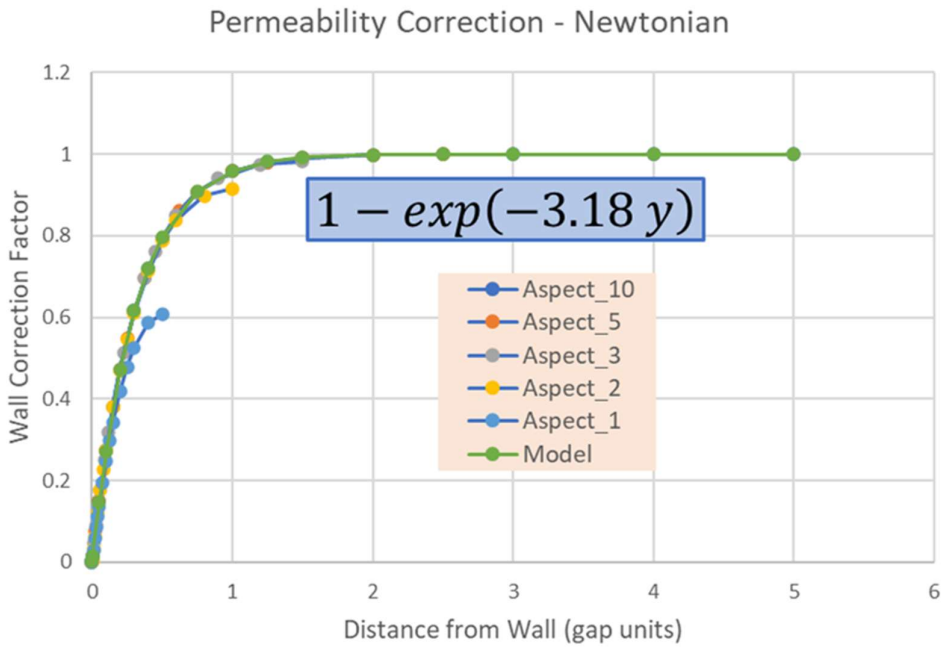

Figure 3 – Comparison of local effective permeability from the series solution for Newtonian flow in rectangular channels of different aspect ratios from 1 to 10. The model shown is an exponential function of the distance from the side wall. The wall correction factor (y-axis) is relative to the permeability of an infinitely wide channel (no side walls).

To a reasonable approximation, the side wall reduces the effective local permeability according to an exponential function of the distance from the side wall.

$$\frac{q(y)}{\nabla p}\mu \approx \frac{H^3}{12}[1-exp(-3.18y)], \quad or \quad \frac{q(y)}{\nabla p}\mu \approx \frac{H_{eff}^3}{12}, \quad H_{eff}(y) = H[1-exp(-3.18y)]^{\frac{1}{3}} \tag{17}$$

For generalized Newtonian liquids, the velocity and thereby the local effective permeability for finite aspect ratio rectangular channels is a more complicated relationship. In general, the local permeability is expected to depend on the wall shear stress as well as the distance from the side wall. Figure 4 (top graphic) shows a computed 2.5-dimensional velocity profile for a Carreau-Yasuda liquid in a 4:1 aspect ratio rectangular channel at a down-channel pressure gradient of 10 kPa/mm. The computation was repeated for a range of down-channel pressure gradient values from 0.1 – 100 kPa/mm. The lower left graphic shows the variation in flow per unit width across the channel for this range. The lower right graphic plots the effective liquid permeability as a function of distance from the side wall for each pressure gradient value. Each curve closely approximates an exponential dependence, i.e., $\frac{q(d)}{\nabla \mathrm{p}} \propto 1 - exp(-\beta d)$, where the factor β varies from about 3.2 for Newtonian behavior and decreases to about 2.0 in the steepest shear-thinning portion of the viscosity curve. Conceivably, in lubrication calculations the exponential factor β could vary directly with the pressure gradient according to 2.5D calculations like those shown in Figure 4. But more likely, an average value in this range would be an effective and reasonably accurate coarse-graining method for most lubrication flows of Generalized Newtonian liquids.

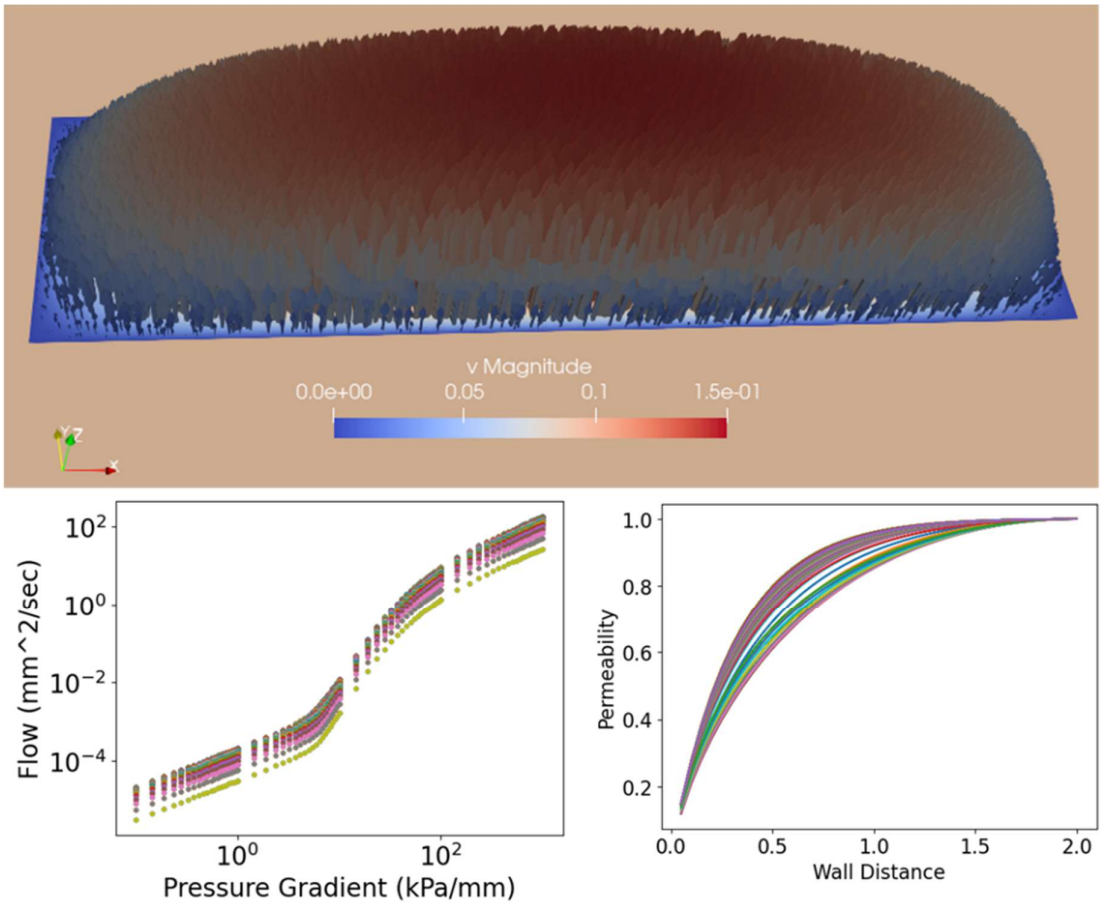

Figure 4: Computed velocity profile (top) from 2.5D FEM calculations for a 4:1 aspect ratio channel and a Carreau-Yasuda fluid ($\frac{dP}{dz} = 10\frac{kPa}{mm}$, η_0=100 Pa-sec, n=0.25, $\lambda = 1$ sec., p=3, η_∞=0.1 Pa-sec). Also shown (lower left) is the variation in flow per unit width across the channel for many imposed pressure gradient values. The lower right graphic plots the effective liquid permeability as a function of distance from the side wall. Each curve represents a particular pressure gradient value from the lower left figure.

4 LUBRICATION FLOW WITH CAPILLARITY

If the lubrication flow contains regions of different phases, such as coating liquid and displaced air, there will be an interface and interfacial forces acting on the flow. Following Roberts et al.[1], we utilize level-set methods to capture interface movement and compute interfacial forces. These forces enter the lubrication momentum balance equations through a continuous surface force (CSF).

$$\boldsymbol{F}_{CSF} = \sigma\kappa\delta(F)\mathbf{n}_{\mathrm{LS}} \approx \sigma\kappa\nabla_{\mathrm{II}}\mathrm{H}(F) \tag{18}$$

The CSF is proportional to surface tension and interface curvature while being weighted with either the level-set delta function or gradient of the level-set Heaviside function, both of which are functions of the level-set distance function, F. The CSF is active only about the level-set interface, which is located at $F = 0$. Roberts et al.[1] reported several calculation results using the Heaviside gradient form while we find the transient calculations to be more productive with

the delta function form. This difference may be the result of using a smooth Heaviside function with a finite width interface zone that we found to be more numerically robust.

For thin channels, the dominant interfacial curvature is expected to be that which points out of the lubrication plane. That is, the surface tangent vector points generally out-of-plane while the curvature vector is in the lubrication plane. The minor curvature component, the in-plane one, has its tangent in the lubrication plane and the curvature vector is out-of-plane.

The out-of-plane curve is taken to be circular arc, intersecting with the upper and lower bounding surfaces at a prescribed contact angle.

$$\kappa_z = \frac{2}{H}\left[-\cos\left(\theta_{sca,U} + \tan^{-1}(n \cdot \boldsymbol{\nabla_{II}} H_U)\right) + \cos\left(\theta_{sca,L} + \tan^{-1}(n \cdot \boldsymbol{\nabla_{II}} H_L)\right)\right] \tag{19}$$

This contact angle could be constant or a function of the flow according to a dynamic wetting correlation or theory.[5]

The in-plane curvature, like Roberts et al.[1] is computed by a separate curvature equation using the level-set field. Numerically, the curvature field is susceptible to spurious wiggles, i.e., oscillating curvature with a wavelength roughly equal to the mesh size. Techniques that aid productive curvature calculation include curvature diffusion, advection of the curvature equation, and modulation of the curvature field far from the liquid-gas interface.

$$\lambda_\kappa \frac{\partial \kappa_{II}}{\partial t} + \lambda_\kappa \langle \boldsymbol{v_{II}} \rangle \cdot \boldsymbol{\nabla_{II}} \kappa_{II} = \mathcal{D} \boldsymbol{\nabla}_{\mathbf{II}}^2 \kappa_{\mathrm{II}} + M(F) \boldsymbol{\nabla}_{\mathbf{II}} \cdot \mathbf{n}_{\mathrm{LS}} \tag{20}$$

Here $\mathcal{D}$ is the curvature diffusion coefficient, $\lambda_\kappa$is an advection time constant, and $M(F)$ is the modulation function which tends toward zero away from the level-set interface.

$$M(F) = 1 \text{ if } |F| < \alpha, \quad M(F) = 0 \text{ if } |F| > 2\alpha, \quad M(F) = 2 - \mathrm{sign}(F)\frac{\mathrm{F}}{2\alpha} \text{ otherwise} \tag{21}$$

Here α is the level-set length scale, i.e., the half-width of the level-set interface. Curvature modulation helps avoid sharp fronts in the curvature field that dramatically slow computations, often by drastically reducing the achievable time step. In addition, using an advection time constant equal to unity, i.e., full advection, enables time steps sometimes as large as 5 times that without curvature advection.

5 CALCULATION RESULTS

Two examples were used to test modified lubrication flow formulations in the fully coupled finite element code Goma.[6] Shell element methods akin to that described by Roberts et al.[1] was deployed. In both examples, quadratic shell elements with a smoothed Heaviside level-set function were used to represent continuous physical properties across the width of the level-set interface. Typically, the level-set length scale, i.e., the half-width of the interface zone, was roughly equal to the lubrication channel gap. Figure 5 shows the Carreau-Yasuda liquid of Figure 2 flowing into a constant thickness mold and around an obstacle. The curvature field (left) is advected and modulated and tends toward zero away from the level-set interface (blue line). The inset shows how the lubrication gap is modified between the lower wall and cylindrical obstacle to account for the drag of the side walls in this channel. The viscosity field (right) shows relatively high viscosity at the leading stagnation point on the obstacle and near the lower wall due to slow flow from drag there. Interestingly, shear-thinning liquids show a locally decreased shear rate and higher viscosity within the level-set

interface zone.

The curvature field computations of Figure 5 were done with curvature advection, modulation, and a diffusion coefficient (~10^3 mm/sec^2) that is large enough to suppress spurious wiggles. The calculation protocol starts with a steady-state calculation of liquid only (i.e., no level-set interface) flowing through the domain. First-order continuation in power-law index is used to proceed from a Newtonian constitutive relation to the Generalized Newtonian model with shear-thinning parameters. Then, a level-set interface is added, and a transient calculation proceeds with identical properties in both phases and zero interfacial tension for about ten timesteps. Lastly, the transient calculation is restarted typically with gas phase properties (density and viscosity) about 1/10th that of the liquid phase and the interfacial tension set to its physical value. Under-relaxation during the Newton's method iterations was used on the first timestep to achieve a converged solution and timestep error is controlled using a variable timestep and an error tolerance of 0.05%.

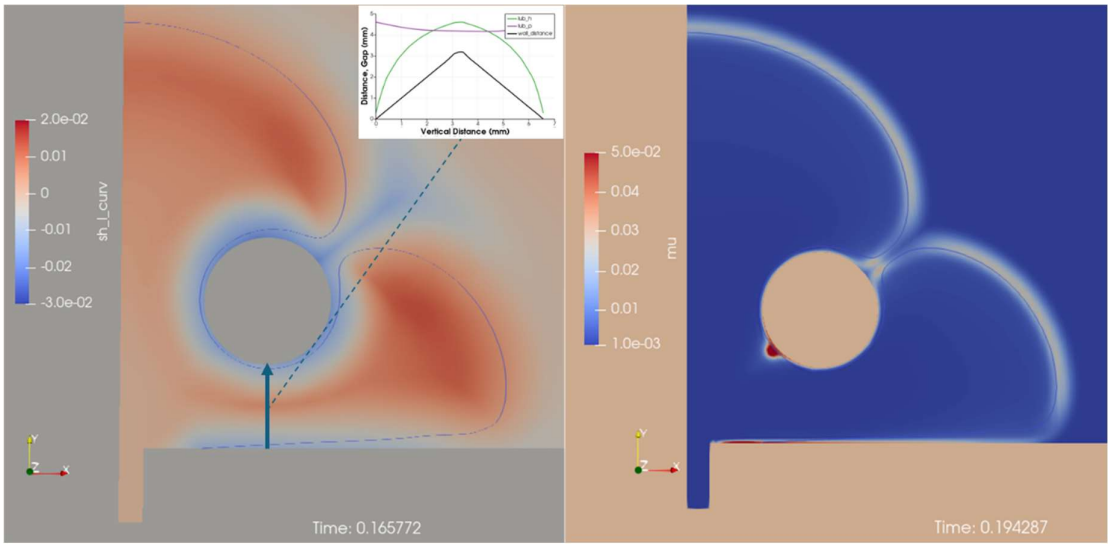

Figure 5: Calculation results of one half of a symmetric flow (10000 mm^3/sec) into a rectangular mold of 5 mm thickness with a cylindrical obstacle whose diameter is 8 mm. The liquid is described by the Carreau-Yasuda model parameters of Figure 2. Both the curvature field (left) and the viscosity field (right) are shown with the level-set interface depicted as a thin blue line. The inset shows the wall distance function (black) and effective lubrication gap (green) below the cylindrical obstacle.

By contrast, the second example (Figure 6) features a Newtonian liquid flowing through a more complicated geometry. Multiple, compact "cross"-shaped obstacles form a flow path for liquid entering from the bottom of the diagram. The cross tips have a radius of 50 um, the same as the channel depth. The aspect ratio of the flow passages between the obstacles approaches unity leading to significant drag from the side walls. Since the liquid is Newtonian, the effective gap relation displayed in (17) was used to quantify the sidewall drag for this situation. The finite element discretization, see magnified views in Figure 6, featured a paved mesh with element sizes in the 3-6 um range. The contact angle of the liquid against the bounding surfaces was set to 90 degrees, so interfacial forces were minimal in this example calculation.

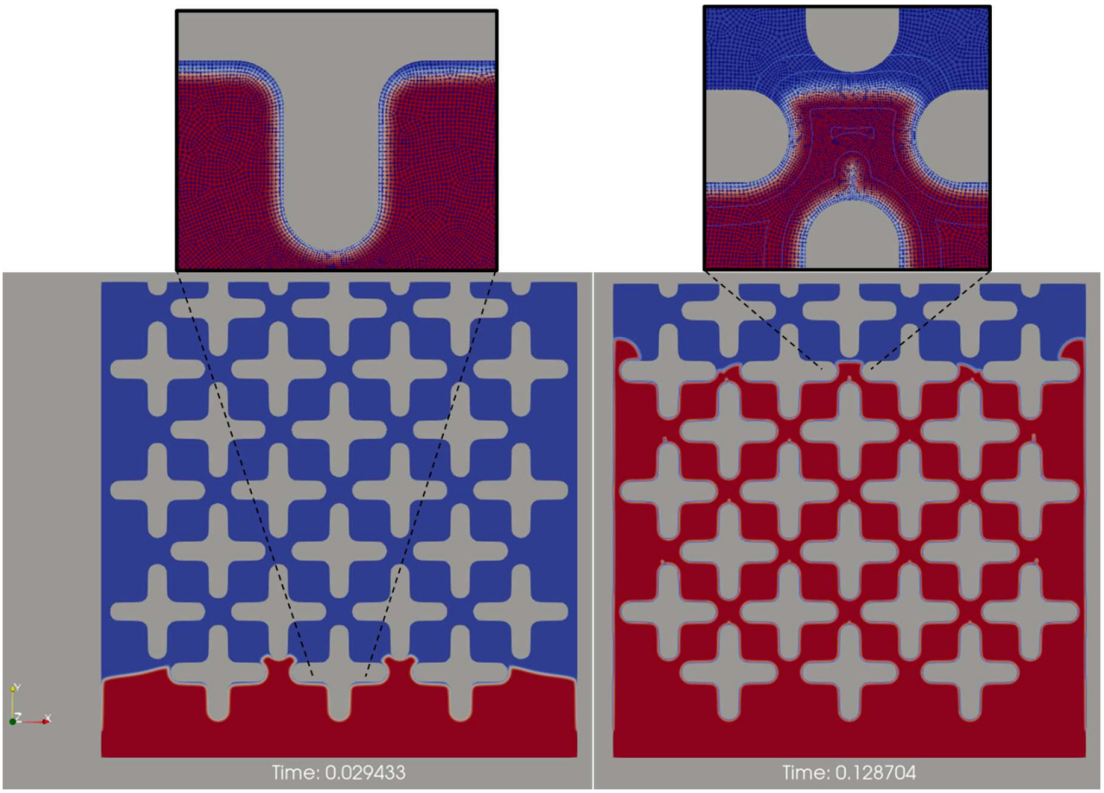

Figure 6: Short time and longer time snapshots of a liquid flowing into a 2.5 mm wide, 0.050 mm deep channel from the bottom at a constant 1.0 mm^3/sec. The coloration refers to viscosity level, so the liquid (water) appears red whereas displaced gas (air) is blue. Two magnified views (top) show the discretization around the obstacle. The right magnification adds 5 level-set field contours across the interface zone. The level-set length scale is 0.0375 mm in this calculation.

One consequence of decreased liquid permeability near the obstacles in the level-set calculation is that liquid is slow to replace gas at these boundaries. The inset in Figure 6 shows a thin layer of gas (blue) which is eventually replaced by liquid (red). But since the level-set interface zone is wider than this layer, interpreting this layer as "gas" may be suspect. In addition, the trailing edges of the cross-shaped obstacles often show small "bubbles" or "fingers" of gas phase that may persist. Usually, finer discretization and more refinement near the trailing edges reduces their occurrence but that carries with it a computational cost. Further calculations with smaller level-set length scales or a sharp interface and experimental flow visualization may clarify the interpretation.

6 SUMMARY

Modifications to Reynolds' lubrication to accommodate shear-thinning rheology and low aspect ratio flow channels have been created and applied to two filling applications. The multi-phase lubrication techniques pioneered by Roberts et al. have been expanded to include modulation and advection of the curvature field in the continuous surface force term. Both advancement areas expand the application space for reduced-order methods in the analysis,

design, and optimization of manufacturing flows via lubrication methods.

Further developments beyond the present work in modifications beyond traditional Reynolds' lubrication seem likely, particularly for manufacturing applications. Lubrication capability for non-isothermal flows due to either imposed temperature differences or heat generated by the flow would be useful, especially for Generalized Newtonian liquids. Continued work on more time-efficient interface movement calculations for multiphase applications would also enable more rapid expansion into more complicated flow geometries and additional physical phenomena.

REFERENCES

[1] Roberts, S.A., Noble, D.A., Benner, E.M., Schunk, P.R., Multiphase hydrodynamic lubrication flow using a three-dimensional shell finite element model. *Computers & Fluids* (2013) **87**:12-25.

[2] Secor, R.B. Analysis and Design of Internal Coating Die Cavities. in *Liquid Film Coating*, edited by Stephan Kistler and Peter Schweizer, Chapman & Hall, (1997).

[3] Bird, R.B., Armstrong, R.C. and Hassager, O. *Dynamics of Polymeric Liquids*. John Wiley. (1987)

[4] Sen A.K. Isothermal creeping flow in rectangular channels. *Industrial & Engineering Chemistry Fundamentals*. (1982) **21**:486-488. doi:10.1021/i100008a031.

[5] Blake, T.D. and Ruschak, K. J. Wetting: Static and Dynamic Contact Lines. in *Liquid Film Coating*, edited by Stephan Kistler and Peter Schweizer, Chapman & Hall, (1997).

[6] Ortiz, Weston 2024, Goma Finite Element Program. accessed May 29, 2024. https://www.gomafem.com.

*Sandia National Laboratories is a multimission laboratory managed and operated by National Technology & Engineering Solutions of Sandia, LLC, a wholly owned subsidiary of Honeywell International Inc., for the U.S. Department of Energy's National Nuclear Security Administration under contract DE-NA0003525.